# Transient Thermal Stresses in Solid-Propellant Grains

A. M. MESSNER* AND D. R. SCHLIESSMANN†
*Aerojet-General Corporation, Sacramento, Calif.*

**This paper describes how finite-difference procedures are used to solve axisymmetric thermal stress problems with the aid of an electronic digital computer. In this solution, elasticity theory is employed in a stress-function formulation that includes the effects of continuously varying temperatures in both the axial and radial directions. Variations of material properties with position are accounted for in a stepwise manner by dividing the solid into zones with independent properties. The finite-difference techniques permit details such as curved boundaries and multimaterial assemblies to be incorporated into the computer program. An extensive experimental test program was developed concurrently with the analysis, and solutions are compared with photoelastic model studies as well as with the measurements made on complete propellant-grain systems. Solutions to several typical propellant-grain problems also are presented in this paper to illustrate the general characteristics of these systems under transient thermal loadings. One of these problems is the transition between two steady-state storage temperatures which is a condition commonly encountered. Results indicate that under this loading the most critical structural condition is usually experienced by the grain at one of the steady-state end conditions.**

## Nomenclature

$E$ = Young's modulus
$f$ = acceleration (gravitational units)
$n, s, \theta$ = orthogonal curvilinear polar coordinates
$r, z, \theta$ = cylindrical polar coordinates
$t$ = thickness, in.
$T$ = change in temperature from cure to ambient, °F
$\alpha$ = linear coefficient of thermal expansion, in./in./°F
$\epsilon, \gamma$ = unit elongation and unit shear
$\nu$ = Poisson's ratio
$\rho$ = density, psi
$\sigma, \tau$ = normal stress and shear stress
$\varphi, \Psi$ = stress functions
$\omega$ = rotational velocity, rad/sec

## Introduction

ROCKET motors are subjected to a variety of thermal environments that produce transient temperature gradients with associated structural problems. These conditions arise from variations in ambient storage temperatures as well as from operational combustion and aerodynamic heating. Motor cases, nozzles, and solid-propellant grains all are susceptible to these conditions, and these effects must be considered during the design of these elements. In addition to structural elements subjected directly to temperature gradients, other components will be influenced indirectly as a result of contact stresses that are transmitted through the composite assemblies.

Mathematical and geometrical complexities associated with these problems preclude the possibility of solving them in complete detail at this time; consequently, some approximations and limitations have been incorporated into this analysis. The first imposed limitation is a restriction to axisymmetric systems. This restriction is not severe because most of the systems of interest contain axial symmetry, and it does make the problems amenable to solution by existing digital computers. Previously reported efforts have included additional approximations such as infinite length[1,2] or have been limited to the analysis of single material systems.[3] The approach taken by Hoyle[3] appears to be most promising, but the amount of effort required to obtain a solution limits it to simple applications. This latter deficiency is overcome by utilizing electronic computers and extending the analysis to include multimaterial assemblies and other, more complicated, boundary conditions.

Before applying an analysis of this type with confidence, it is necessary to establish the validity of the results. For this reason, a concurrent experimental test program was conducted. Photoelastic model studies were undertaken to check steady-state solutions, and instrumented propellant-grain systems were used to obtain transient data. Propellant grains are well suited to this role since their modulus of elasticity varies over several orders of magnitude in the temperature range from +100°F to −100°F. Instrumentation problems are not severe at these moderate temperatures, and transient thermal gradients persist for several hours because of the high heat capacity and low thermal conductivity of the propellant.

## Analysis

The analysis is made within the framework of infinitesimal elasticity theory; consequently, it is subject to all the limitations and assumptions of this theory. In particular, the material is assumed to be an isotropic elastic solid, and the magnitude of the strains, rotations, and displacements are assumed to be small. Also, temperature-dependent nonhomogeniety is accounted for incrementally by dividing the structure into a number of zones and assigning each zone a specific set of mechanical properties.

A stress-function formulation for axisymmetric solids attributed to Hoyle[3] was used in this analysis. Two stress functions $\varphi$ and $\Psi$ are employed in this formulation given in Eqs. (1–6). A different sign convention is used for the stress functions than that used by Hoyle in order to conform to the earlier equations derived by Southwell.[4] Along curved boundaries it has been found advantageous to use orthogonal curvilinear coordinates. The formulation transformed into this coordinate system is given in Eqs. (7–10):

$$\frac{\partial^2\varphi}{\partial r^2} - \frac{1}{r}\frac{\partial\varphi}{\partial r} + \frac{\partial^2\varphi}{\partial z^2} = 0 \tag{1}$$

$$\frac{\partial^2\Psi}{\partial r^2} - \frac{1}{r}\frac{\partial\Psi}{\partial r} + \frac{\partial^2\Psi}{\partial z^2} = \frac{\partial^2\varphi}{\partial z^2} + \frac{E\alpha}{1-\nu} r \frac{\partial T}{\partial r} \tag{2}$$

Presented as Preprint 64-233 at the 1st AIAA Annual Meeting, Washington, D. C., June 29–July 2, 1964; revision received March 8, 1965.

* Design Engineer, Structural Analysis Program, Solid Rocket Structures Division. Member AIAA.

† Design Engineer, Structural Analysis Program, Solid Rocket Structures Division.

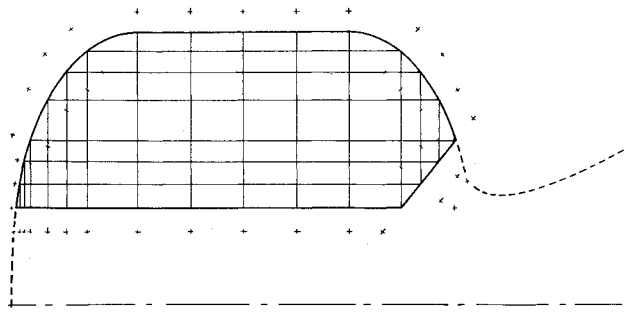

**Fig. 1 A finite-difference grid.**

$$\sigma_r = \frac{1}{r}\left[\frac{\partial\varphi}{\partial r} + \frac{\partial\Psi}{\partial r}\right] - \frac{1}{r^2}\left[\Psi + (1-\nu)\varphi\right] - \frac{1}{8}\frac{3-2\nu}{1-\nu}\rho\omega^2r^2 - \frac{E\alpha T}{1-\nu} \quad (3)$$

$$\sigma_\theta = \frac{\nu}{r}\frac{\partial\varphi}{\partial r} + \frac{1}{r^2}\left[\Psi + (1-\nu)\varphi\right] - \frac{1}{8}\frac{1+2\nu}{1-\nu}\rho\omega^2r^2 - \frac{E\alpha T}{1-\nu} \quad (4)$$

$$\sigma_z = -\frac{1}{r}\frac{\partial\Psi}{\partial r} - \frac{1}{2}\frac{\nu}{1-\nu}\rho\omega^2r^2 + \rho f_z Z \quad (5)$$

$$\tau_{zr} = (1/r)(\partial_\Psi/\partial z) \quad (6)$$

$$\frac{\partial^2\varphi}{\partial n^2} - \frac{1}{r}\sin(z,n) - \frac{r}{R_1}\frac{\partial\varphi}{\partial n} + \cos(z,n)\frac{\partial\varphi}{\partial s} + \frac{\partial^2\varphi}{\partial s^2} = 0 \quad (7)$$

$$\frac{\partial^2\Psi}{\partial n^2} - \frac{1}{r}\left[\sin(z,n) - \frac{r}{R_1}\frac{\partial\Psi}{\partial n} + \cos(z,n)\frac{\partial\Psi}{\partial s}\right] + \frac{\partial^2\Psi}{\partial s^2} = \frac{\partial^2\varphi}{\partial z^2} + \frac{E\alpha}{1-\nu}r\left[\sin(z,n)\frac{\partial T}{\partial n} + \cos(z,n)\frac{\partial T}{\partial s}\right] \quad (8)$$

$$\sigma_n = \left[\rho f_z Z - \frac{1}{2}\frac{\nu}{1-\nu}\rho\omega^2r^2\right]\cos^2(z,n) - \frac{\cos(z,n)}{r}\frac{\partial\Psi}{\partial s} + \sin(z,n)\frac{\partial(\Psi/r)}{\partial n} + \sin^2(z,n)\left[\frac{1}{r}\frac{\partial\Psi}{\partial r} - \frac{(1-\nu)\varphi}{r^2}\right] - \frac{1}{8}\frac{3-2\nu}{1-\nu}\rho\omega^2r^2\sin^2(z,n) - \sin^2(z,n)\frac{E\alpha T}{1-\nu} \quad (9)$$

$$\tau_{ns} = -\left[\rho f_z Z - \frac{1}{2}\frac{\nu}{1-\nu}\rho\omega^2r^2\right]\sin(z,n)\cos(z,n) + \frac{\sin(z,n)}{r}\frac{\partial\Psi}{\partial s} + \cos(z,n)\frac{\partial(\Psi/r)}{\partial n} + \sin(z,n)\left\{\left[\frac{1}{r}\frac{\partial\varphi}{\partial r} - \frac{(1-\nu)\varphi}{r^2}\right] - \frac{1}{8}\frac{3-2\nu}{1-\nu}\rho\omega^2r^2\right\} - \sin(z,n)\cos(z,n)\frac{E\alpha T}{1-\nu} \quad (10)$$

A solution to any given problem is obtained by solving Eqs. (7) and (8) in such a manner that the specific boundary conditions also are satisfied. In general, these boundary conditions involve combinations of Eqs. (9) and (10), as well as integrals of these expressions around the boundaries. Although it is theoretically possible to solve these problems analytically, practical considerations preclude the possibility of solving any but the simplest problems without recourse to some numerical procedure. For this reason, a finite-difference numerical technique has been used in this analysis, and the resulting equations have been programed for solution on a digital computer.

Digital computers are fast and economical when performing routine arithmetic operations. However, extensive programing is required for complex logic decisions by the computer. This is the reverse of the situation encountered in a hand solution. Because of this characteristic of digital computers, established numerical procedures need to be modified if the computers are to be used effectively. The most significant difference in this routine from past efforts concerns the use of a nonuniform finite-difference grid, intersections of which define the geometry of the solid. Fictitious grid points are employed but are located along normals to the boundary of the solid rather than along extensions of the existing grid as is the method used in manual solutions. This procedure results in an extensive amount of arithmetic but yields a consistent treatment that can be programed for computer operation with a minimum of logic decisions. All of the fictitious points and all of the required finite-difference equations are generated by the computer. A typical geometry and finite-difference grid is shown in Fig. 1.

Differential Eqs. (1–10) are converted to finite-difference form by expanding the functions in a Taylor series. Consider the stress function $\varphi$ and its value a finite interval to the right and to the left of the origin. The Taylor series expansions are

$$\varphi_R = \varphi_0 + h_R\frac{\partial\varphi}{\partial z} + \frac{h_R^2}{2}\frac{\partial^2\varphi}{\partial z^2} + \ldots$$

$$\varphi_L = \varphi_0 - h_L\frac{\partial\varphi}{\partial z} + \frac{h_L^2}{2}\frac{\partial^2\varphi}{\partial z^2} - \ldots$$

$h_R$ and $h_L$ refer to the finite intervals to the right and left, respectively. When derivatives higher than the second order are neglected and these equations are solved for $\partial\varphi/\partial z$ and $\partial^2\varphi/\partial z^2$, the following expressions are obtained:

$$\frac{\partial\varphi}{\partial z} = \frac{1}{h_L(h_L+h_R)h_R}\left[h_L^2\varphi_R - (h_L^2 - h_R^2)\varphi_0 - h_R^2\varphi_L\right]$$

$$\frac{\partial^2\varphi}{\partial z^2} = \frac{2}{h_L(h_L+h_R)h_R}\left[h_L\varphi_R - (h_L+h_R)\varphi_0 + h_R\varphi_L\right]$$

Similar expansions in the radial, normal, and surface direc-

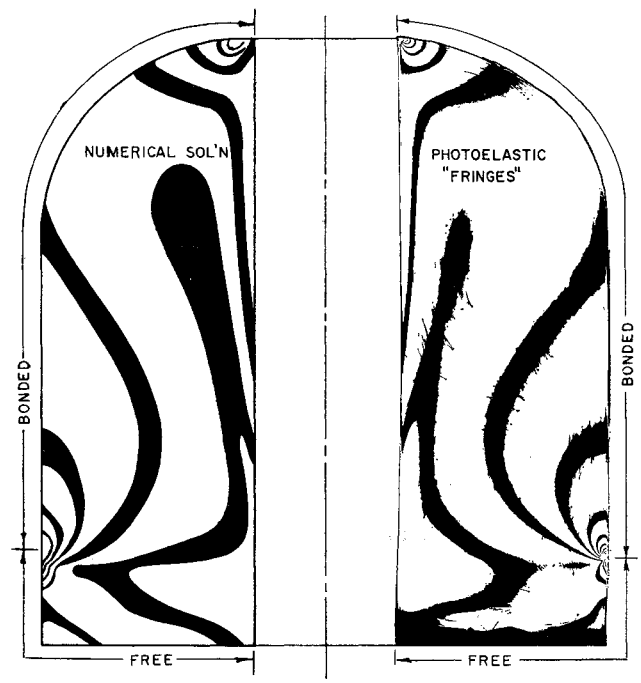


**Fig. 2 Comparison of numerical and photoelastic stress contour.**

tions lead to the finite-difference equations for the derivative with respect to these coordinates.

The two stress functions at each grid intersection point are the unknowns, and the finite-difference form of Eqs. (1) and (2) at each real grid point are the corresponding algebraic equations. At the boundaries of the solid, two additional equations such as a normal load and a shear-stress equation must also be satisfied. These additional conditions are matched by the fictitious unknowns resulting in a complete set of simultaneous equations.

The particular boundary conditions employed are usually simple combinations of Eqs. (9) and (10), but the intermaterial boundary equations are sufficiently complex to warrant further explanations. At an interface between two dissimilar materials, fictitious unknowns are associated with each material, resulting in four additional unknowns at each contacting node. The four conditions that must be satisfied are the contact normal and shear stresses, which must be equated for both materials, and the two components of displacement which also must be equated. Because displacements are difficult to specify in a stress-function approach, an indirect procedure was adopted. On these surfaces, it was convenient to specify derivatives of the displacements rather than the actual displacements. Specification of the displacement derivatives at all points of contact insures that the displacements, which are their integrals, are also matched everywhere. The four intermaterial conditions that are applied at the interface between materials $A$ and $B$ are given in the following equations:

$$\begin{aligned} (\sigma_n)_A &= (\alpha_n)_B & (\tau_{ns})_A &= (\tau_{ns})_B \\ (\partial u_n/\partial s)_A &= (\partial u_n/\partial s)_B & (\partial u_s/\partial s)_A &= (\partial u_s/\partial s)_B \end{aligned} \tag{11}$$

Subscripts $A$ and $B$ in these equations refer to the two materials, and $u_n$ and $u_s$ are displacements normal and tangential to the surface, respectively. The displacement derivatives are given in terms of the stress functions in Eqs. (12) and (13):

$$\frac{\partial u_n}{\partial s} = \frac{1+\nu}{rE}\left\{[\sin^2(z,n) - 1 + \nu]\cos(z,n)\frac{\partial\varphi}{\partial n} + [\cos^2(z,n) + 1 - \nu]\sin(z,n)\frac{\partial\varphi}{\partial s} + \cos(z,n)\frac{\partial\varphi}{\partial n} + \sin(z,n)\frac{\partial\Psi}{\partial s}\right\} + \sin(z,n)\cos(z,n)\frac{1+\nu}{E}\times\left\{-\frac{1}{r^2}[\Psi + (1-\nu)\varphi] - \frac{3}{8}\frac{1-2\nu}{1-\nu}\rho\omega^2r^2 - \rho f_z Z\right\} + \frac{\nu}{E}\rho f_z r + \sin(z,n)\cos(z,n)\left[-\alpha T\frac{1+\nu}{1-\nu}\right] \tag{12}$$

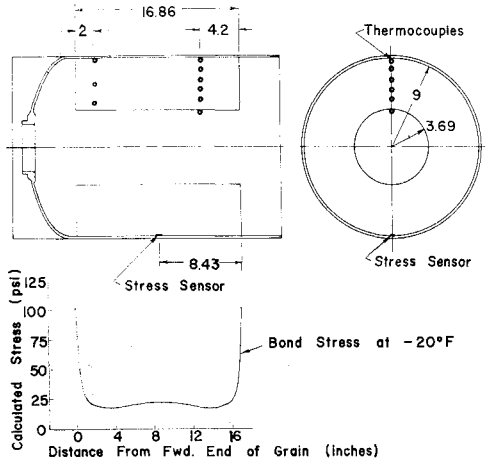


**Fig. 3 Experimental grain model configuration.**

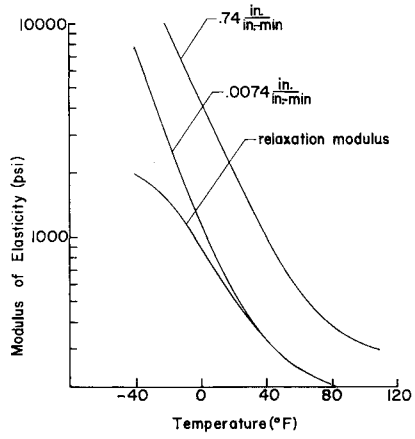


**Fig. 4 Modulus of elasticity vs temperature.**

$$\frac{\partial u_s}{\partial s} = \cos^2(z,n)\frac{1}{E}\left\{-\frac{1+\nu}{r^2}[\Psi + (1-\nu)\varphi] - \frac{3}{8}\frac{1-\nu-2\nu^2}{1-\nu}\rho\omega^2r^2 - \nu\rho f_z Z\right\} + \frac{\sin^2(z,n)}{E}\rho f_z Z + \frac{1+\nu}{rE}\left[-\sin(z,n)\frac{\partial\Psi}{\partial n} + \cos\frac{\partial\Psi}{\partial s}\right] + \frac{1+\nu}{rE}[\cos^2(z,n) - \nu]\left[\sin(z,n)\frac{\partial\varphi}{\partial n} + \cos(z,n)\frac{\partial\varphi}{\partial s}\right] + \frac{1+\nu}{1-\nu}\sin^2(z,n)\alpha T \tag{13}$$

Input effort has been minimized and the computer used to generate all equations and solve the problem. A Gaussian elimination procedure is used to solve the simultaneous equations. This direct method of solution avoids the problems of convergence encountered in relaxation or iteration techniques.[3,5]

## Experimental Evaluation

The computer was first applied to simple plane-strain and steady-state problems with available analytic solutions, but these solutions were soon exhausted, and recourse was made to experimental procedures. Photoelastic model studiee were made to determine the validity of the steady-state results, and propellant-grain systems were used to evaluate transient conditions. In the photoelastic evaluation, an axisymmetric thick cylinder with a curved head was bonded to a metal case and subjected to a simulated steady-state temperature change.[6] Stresses were generated by the differential expansion of the case and the cylinder which had dissimilar coefficients of thermal expansion.

The photoelastic stress patterns obtained using this technique were frozen in the three-dimensional model, subsequently sectioned, and analyzed. In this manner detailed stress distributions were obtained for comparison with numerical results. The experimental results agreed closely with the theoretical evaluations as indicated by the similar stress patterns for the two methods of analysis shown in Fig. 2. These studies established the validity of the analysis for

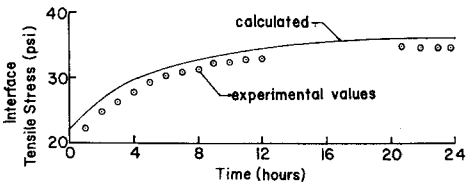


**Fig. 5 Tensile stress vs time during cooling from steady stack −20° to −40°F.**

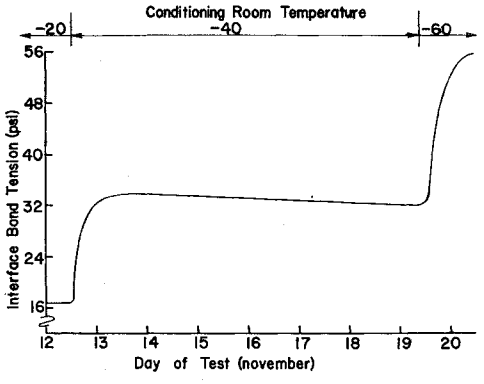


**Fig. 6 Measured bond tension vs time.**

elastic systems subjected to steady-state thermal stresses; however, a more elaborate test was still needed to check the method in transient conditions and with propellant materials.

Next, an experimental evaluation of a transient temperature gradient condition was attempted with a subscale propellant-grain system. Two identical thick cylinders of propellant were cast into aluminum cases and instrumented as shown in Fig. 3. One of the cylinders contained all the thermocouples whereas the other was instrumented with bond-stress sensors and inner-bore measuring devices. The bond-stress sensors were imbedded between the propellant and the case at points where the numerical solutions indicated that a uniform stress distribution would be obtained. These test models were subjected to a series of 20°F incremental temperature changes. Several cycles were made over the temperature range from 110° to −60°F. During each cycle, bond stresses and temperatures were recorded continuously, and inner-bore profile measurements were made at each temperature increment.

The propellant used in the test models is not a perfectly elastic solid but a viscoelastic one with time-dependent mechanical properties. However, such a system can be analyzed as an elastic solid provided that an effective modulus appropriate for the particular loading rate is used. The sensitivity of the modulus of elasticity to strain rate is shown in Fig. 4, where uniaxial tensile test data for different strain rates are plotted. It was not practical to perform these tests at the same strain rates that are encountered by the propellant grains under the thermal loads, and, for this reason, appropriate shift factors[7] were used to obtain the required slow-rate relaxation modulus shown in Fig. 4.

A comparison of the transient test data with numerical solutions indicates that the data correlated reasonably well.

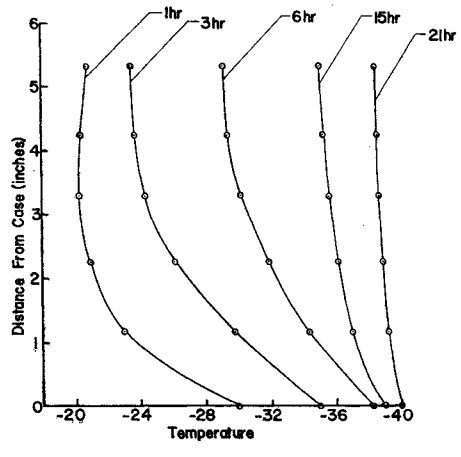


**Fig. 7 Temperature distribution through propellant web from thermocouple measurements.**

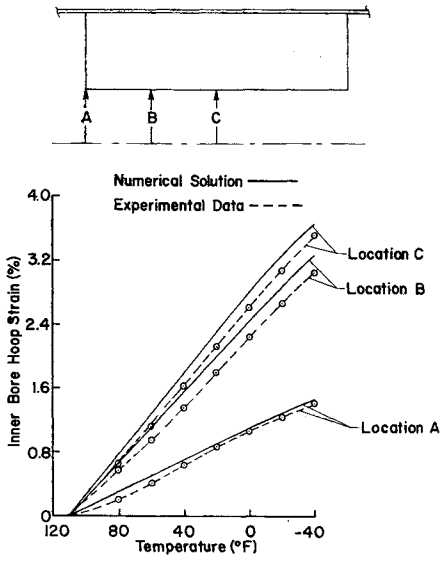


**Fig. 8 Inner-bore hoop strain vs temperature for three locations along bore.**

Typical of the bond-stress data is the −20° to −40°F step shown in Figs. 5–7. These data are plotted in Fig. 5 along with the numerical solutions for this condition. The higher numerical results are attributed to the approximate manner in which the modulus was estimated. The data of Fig. 6 indicate that the effective modulus of the propellant continues to decrease with time for several days after steady-state temperatures are reached as evidenced by the decay in bond tension with time. This viscoelastic nature of the propellant did not have any measurable effect on the inner-bore strains that remained constant after steady-state temperatures had been reached. These inner-bore steady-state strains are compared with the numerical results in Fig. 8 which indicate that good correlation was achieved. The test cylinders finally were subjected to a −85°F environment that produced a bond failure. Prior to the failure, stresses of 60 psi were recorded but, as the unbonded region progressed from the end of the cylinder toward the center, the stress increased. The test was stopped when the unbonded region extended to the stress sensor, at which time a reading of 400 psi had been reached. This stress could not be checked analytically because of the irregular nature of the unbonded region; however, the data indicate that the severe stress peaks predicted for the ends of the bonds actually exist.

## Applications

Although the experimental evaluation of this numerical analysis is still incomplete, the accurate correlation obtained permits the application of the numerical analysis to practical propellant-grain problems with reasonable certainty. The solutions to two such problems follow to illustrate the characteristics of these systems.

The first problem concerns a rocket motor (Fig. 9), which has been stored at a controlled temperature of +60°F that is to be exposed to a 65 mph wind at −30°F for several hours.

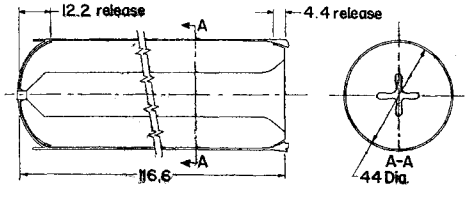


**Fig. 9 Configuration of example problem 1.**

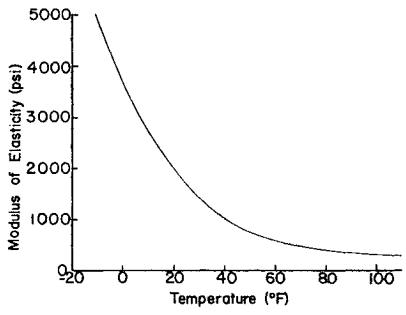


**Fig. 10 Relaxation modulus of propellant vs temperature.**

The problem is to determine the structural effect on the propellant grain. The propellant in this motor has been cured at 110°F and is assumed to be stress-free at this temperature. The temperature distributions and propellant-relaxation-modulus data are shown in Figs. 10 and 11. At each fixed time, there is a variation of modulus with radius that must be converted into a number of finite steps. This incremental modulus characterization is shown in Fig. 11. The temperature distribution is input to the computer as analytic expressions in terms of powers of the radius for each of the six zones. This procedure is repeated for each fixed time selected, and solutions are obtained on the computer for each of these problems. Each solution contains a wealth of data showing the complete stress-strain distribution in the motor. Of these data, only the maximum stresses and strains are of interest, and, in this particular problem, only the maximum inner-bore strain and the maximum bond tension are pertinent. Next, this bond tension and inner-bore strain are plotted as functions of time along with the corresponding failure characteristics of the propellant at the respective temperatures. These plots have been constructed for this motor and are shown in Fig. 12.

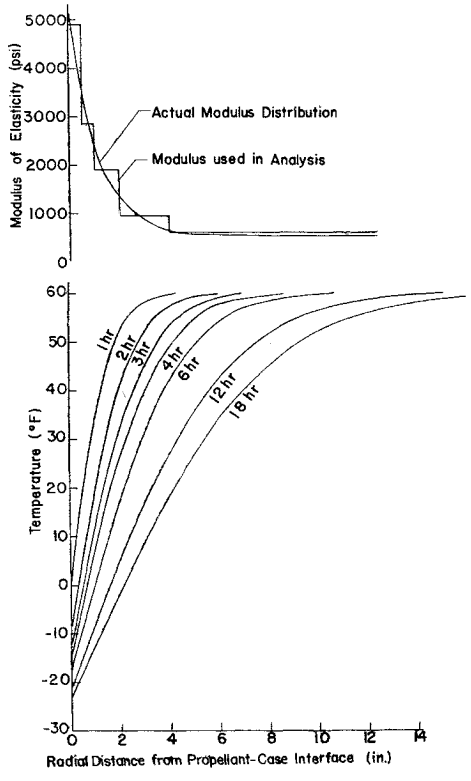


**Fig. 11 Modulus of elasticity after 12 hr and calculated temperature vs propellant depth for motor in −30°F environment. Initial motor temperature −60°F and wind velocity −65 mph.**

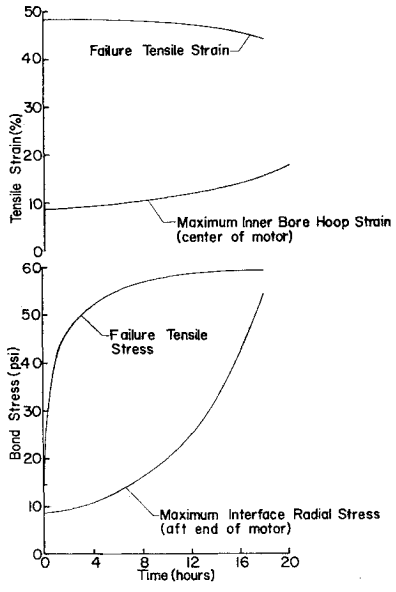


**Fig. 12 Strained stress vs time for motor stored at 60°F exposed to −30°F in 65 mph wind.**

A solution to another transient thermal problem is shown in Fig. 13. This problem was encountered in a motor that was stored at −75°F until a steady-state temperature was reached. Subsequent to this conditioning, the motor was placed in a 200°F oven until a steady-state condition was again achieved. For this particular problem, thermocouples were imbedded in the propellant, and experimental temperature data were obtained. Theoretical temperature distributions also were calculated and used to interpolate between the experimental data points. Bond failure was the only concern in this motor; consequently, the maximum bond stress and corresponding failure characteristics are shown as functions of time in Fig. 13.

## Summary and Conclusions

The original contention that an automated version of the finite-difference procedures utilizing a digital computer would overcome the difficulties encountered in relaxation approaches to these problems appears to have been substantiated. Solutions have been obtained to a wide variety of problems, and neither curved boundaries nor mixed boundary conditions have posed any particular difficulties. The results

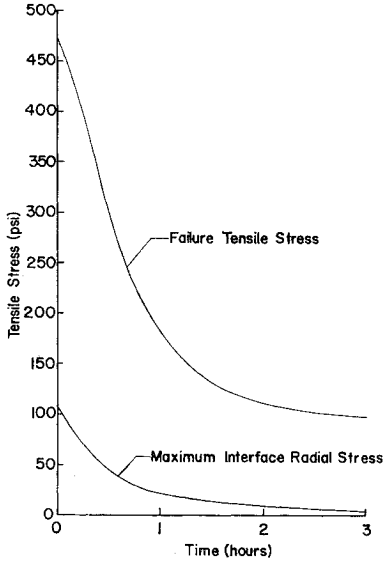


**Fig. 13 Tensile stress vs time for motor stored at −75°F and then exposed to 200°F.**

obtained have been checked against known solutions and a limited number of photoelastic and experimental test models. In all instances adequate correlation was achieved.

In the particular case of environmental conditioning propellant grains, maximum stresses and strains invariably occur at the initial or final steady-state condition. This does not eliminate these systems from consideration, however, because not all loadings are maintained until steady-state temperatures are achieved as in the first example problem. Although the failure criteria used in this analysis do not include time- or path-dependent characteristics, some propellants possibly may exhibit such properties. If such phenomena are anticipated, a critical condition could exist at an intermediate temperature, and a transient analysis would be required.

This study has been oriented specifically toward propellant-grain problems, but no such limitation is inherent in the techniques described. The computer program can be applied without modification to other axisymmetric components such as nozzles, nose cones, and turbine rotors. Loads other than thermal stresses can also be analyzed because the formulation includes surface pressure, shears, and body forces generated by either axial or rotational accelerations. Experimental data for these problems are not very extensive, however, and the analysis must be used with caution until adequate substantiating data become available.

## References

[1] Strub, R. A., "Distribution of mechanical and thermal stresses in multi-layer cylinders," Trans. Am. Soc. Mech. Engrs. **75**, 73 (1953).

[2] Matsumura, T., "A contribution to the theory of thermal stresses in a long hollow cylinder," Kyoto Imperial Univ., College of Engineering Memoirs **3**, 61 (1923).

[3] Hoyle, R. D., "Transient temperature stresses in axially symmetric systems with special attention to a rotor of a steam turbine," Proc. Inst. Mech. Engrs. (London) **169**, 553 (1955).

[4] Southwell, R. V., *Relaxation Methods in Theoretical Physics* (Oxford University Press, London, 1956).

[5] Baines, B. H. and Hoyle, R. D., "Thermal stresses in elastic axially symmetrical bodies," J. Mech. Eng. Sci. **4**, 111 (1962).

[6] Sampson, R. C., "A three-dimensional photoelastic method for analysis of differential contraction stresses," Exp. Mech. **3**, 225 (1963).

[7] Williams, M. L., Landel, R. F., and Ferry, J. D., "The temperature dependence of relaxation mechanisms in amorphous polymers and other glass forming liquids," Proc. Fourth U. S. Natl. Congr. Appl. Mech. **2**, 3701 (1955).

JULY-AUG. 1965 J. SPACECRAFT VOL. 2, NO. 4

# Design of a Versatile Liquid-Fluorine/Liquid-Hydrogen Upper Stage

GEORGE C. GOLDBAUM* AND JOHN B. DOUGLASS†
*Douglas Aircraft Company, Inc., Santa Monica, Calif.*

**A design is presented of a fluorine-hydrogen upper stage that can be developed and produced with current technologies and which is applicable to boosters ranging in size from small to large. When used in an upper stage, a propellant combination of fluorine and hydrogen gives the highest performance of any state-of-the-art propellant. Detailed sizing studies show that an upper stage of 30,000-lb propellant capacity, powered by a 35,000-lb-thrust $F_2$-$H_2$ engine, will provide near-maximum payload capability for boosters from small to large class vehicles for missions from low orbit to escape. The lightest, strongest, and most easily insulated structural configuration is a load-bearing outer shell of aluminum honeycomb with spherical fluorine and hydrogen tanks suspended internally. Detailed analysis of one insulation method, layers of aluminized mylar separated from each other by the natural crinkling of the material, showed that boiloff would be less than 21 lb of fuel to coast to the 24-hr satellite altitude.**

## Introduction

THE current stable of the Nation's space vehicles comprises many boosters and combinations of upper stages. Depending on the mission to be performed, the booster to be used, and even the launch site, a variety of upper stages is required. As the national space program evolves, extensive mission capability for exploration of the solar system will be required. Mission velocity requirements will rise above 40,000 fps and payload weights will, necessarily, increase as a result of shielding, power, and communications requirements.

If economy were not demanded, it would be possible to satisfy mission extensions by simply building ever-larger boosters. Alternatively, the capabilities of existing boost systems can be extended to cover the required high-energy missions by a properly sized, high-energy upper stage. The desirable requirements for this stage should be: highest available performance capability, thrust level and propellant capacities optimized for general applicability to missions ranging from low earth orbit to high-energy escape, efficient stage design with provisions for restart and operation after "many" hours of zero "$g$" coast, economical development and operations costs, and growth potential for unidentified future manned and unmanned missions.

Presented at the 1st AIAA Annual Meeting, Washington, D. C., June 29–July 2, 1964; revision received October 19, 1964. The technology and systems studies, integrated into this system design, were conducted by the Missile and Space Systems Division, Douglas Aircraft Company, Inc., under company-sponsored research and development funds.

* Director, Advance Launch Systems, Missiles and Space Systems Division.

† Advance Project Engineer, Missiles and Space Systems Division.